Open Geosci. 2019; 11:866–876 **DE GRUYTER**

Research Article

Ying Liu* and Hui Yue

Remote Sensing Monitoring of Soil Moisture in the Daliuta Coal Mine Based on SPOT 5/6 and Worldview-2

https://doi.org/10.1515/geo-2019-0067 Received Jan 19, 2019; accepted Aug 27, 2019

Abstract: To understand the influence of underground mining disturbances on the shallow soil moisture in the Daliuta coal mine, remote sensing monitoring of the temporal and spatial evolution of surface soil moisture and the influence of mining on multi-source, multi-temporal and high spatial resolution remote sensing data were carried out. The scale effect of monitoring the soil moisture at different scales was analyzed using the Scaled Soil Moisture Monitor Index (S-SMMI). In this paper, SPOT 5/6 and Worldview-2 were used as the data source and mainly made up two aspects of the research: 1) based on the three SPOT data sets with the use of S-SMMI from different angles from the Daliuta mine from nearly three years of soil moisture temporal and spatial changes, the results show that the perturbation has a negative effect on the shallow soil moisture in the Daliuta coal mine, and average soil moisture of the mining area is smaller than the nonmining area, but the surface ecological construction has effectively improved the impact of the underground mining disturbance on the surface soil moisture. 2) the scale conversion of Worldview-2 data was carried out based on the resampling method. S-SMMI was used to analyze the scale effect of soil moisture monitoring at different scales. The results show that the difference between the soil moisture is only 0.0016 during the conversion process of 2 m-30 m.

Keywords: soil moisture, remote sensing monitoring, S-SMMI, scale effect, Daliuta

Email: liuying712100@163.com

Hui Yue: Key Laboratory of Mine Geological Hazards Mechanism and Control, Yanta Road, Xi'an, China, 710054; Xi'an University of Science and Technology, College of Geomatics, Yanta Road, Xi'an, China, 710054; Email: 13720559861@163.com

1 Introduction

Soil moisture (SM) is a physical quantity that indicates the degree of soil dryness and wetness in a certain depth [1–4]. Soil moisture is an important factor in studying the conversion of ground gas energy and water cycle, plays an important role in various processes and feedback loops within the Earth system and also an important indicator for remote sensing drought monitoring [5–10]. Soil moisture can be obtained by field instrumental measurements or remote sensing estimates. With the rapid development of Earth observation technology, the field of soil moisture remote sensing has developed greatly in the past few decades [11, 12]. Thus, researchers have gradually shifted their attention to monitoring soil moisture by using remote sensing techniques [13-15]. Currently, SM is an important indicator of remote sensing monitoring. Based on the multi-band information of visible light, near infrared, thermal infrared and microwave, many models and methods for soil moisture remote sensing monitoring are proposed [16-18]. It was developed by establishing relationships between SM and soil reflectivity or surface temperature/vegetation coverage and soil thermal properties [19, 20].

Traditional SM acquisition methods mainly include single-point based or specific location measurements. The direct and most accurate method is the gravimetric method [21, 22]. The original soil moisture content can be confirmed by the change of soil quality. However, this method is destructive and cannot be reproduced. Moreover, this method needs the support of human sampling and laboratory equipment [9]. Today, soil moisture measuring instruments have been further developed. For example, Time Domain Reflectometry (TDR), neutron probes and gamma ray scanners are subsequently used to indirectly measure the SM [23]. However, these methods are based on point measurements, and cannot be used as data for regional or surface soil moisture. With the rapid development of remote sensing technology, remote sensing monitoring of soil moisture has become the focus of research. There methods were established for retrieving soil



^{*}Corresponding Author: Ying Liu: Key Laboratory of Mine Geological Hazards Mechanism and Control, Yanta Road, Xi'an, China, 710054; Xi'an University of Science and Technology, College of Geomatics, Yanta Road, Xi'an, China, 710054;

moisture based on the relationship between surface soil moisture and satellite-derived land surface parameters. The spectral feature space method based on NIR-Red has been further extended and applied because of its simplicity and ease of operation. There are two kinds of soil moisture monitoring indices based on NIR-Red spectral characteristic space. One is based on the vertical distance between any point in the characteristic space and the straight line passing through the origin (which is perpendicular to the soil baseline), such as Perpendicular Dryness Index (PDI), the Modified Perpendicular Drought Index (MPDI), etc. The second is to use the distance from any point in the characteristic space to the origin directly (such as shortwave infrared soil moisture index, soil moisture monitoring index (SMMI), etc.) to characterize the soil moisture status in the study area.

Based on the energy balance equation, the principles of the thermal inertia method and the thermal inertia of remote sensing imaging are systematically summarized, and the concept of Apparent Thermal Inertia is proposed to make the visible light and near-infrared channel reflectivity provided by satellite. And thermal infrared radiation temperature difference to calculate thermal inertia and estimate soil moisture becomes possible [24, 25]. In recent years, the drought monitoring index derived from the vegetation index has been further expanded and applied because of its ease of use. Moran et al. [26] proposed the evapotranspiration index-water deficit index (WDI), which can monitor the surface vegetation coverage and part of the vegetation coverage. Based on the water loss index, the concept of Temperature Vegetation Dryness Index (TVDI) was proposed by Sandholt [15] in 2002. The algorithm is only required to rely on remote sensing image data, and the normalized difference vegetation index (Normalized Difference Vegetation Index, NDVI) and surface temperature are normalized. Ghulam [27] proposed a soil moisture monitoring model based on surface spectral characteristics—Perpendicular Dryness Index (PDI). This method directly replaces the previous Normalized Difference Vegetation Index (NDVI) and albedo (Albedo) with spectral features, which is simple and effective. However, PDI is more suitable for drought monitoring in bare soils, and monitoring accuracy in the vegetation area will be affected. In response to this problem, Ghulam [28] introduced vegetation coverage and proposed a Modified Perpendicular Drought Index (MPDI). Zhang [29] used HyMap and Hyperion images to study the Mount Lyell mining area in Australia and the Dexing copper mine in China and proposed VII (Vegetation Inferiority Index, VII) and WDI (Water Absorption Disrelated Index, WDI). The results show that the vegetation is better than the Traditional Vegeta-

tion in Monitoring Vegetation Growth. The index NDVI and WDI can be used to identify hematite in sparse vegetation covered areas. Amani [30] constructed two trigonometric soil moisture indices (Triangle Soil Moisture Index, TSMI) and enhanced the triangular soil moisture index (Modified Triangle Soil Moisture Index, MTSMI), based on the Landsat 8 NIR-Red spectral feature space. Amani compared it with the real data and considered that the two exponents were retrieved. Soil moisture is highly correlated with 5 cm deep soil moisture.

Throughout the aforementioned studies, a variety of indicator factors were initially used to establish a large number of soil moisture inversion models. The indicators include thermal inertia, surface temperature, vegetation index, backscatter coefficient, and brightness temperature, etc. Later, research began with active and passive remote sensing. The data were combined to invert the soil moisture. Many scholars verified the different drought monitoring indexes based on the two-dimensional spectral feature space. The results showed that they have different applicability to large-scale remote sensing drought monitoring [31].

The study of the Shendong Mining Area mostly analyses the changes of vegetation and soil moisture in the mining area to evaluate the environmental quality of the mining area in the macroscopic domain. In recent years, many scholars have conducted research on the Daliuta mine, but previously, remote monitoring on the surface environment of the Daliuta Coal Mine had not been completed. The following problems still exist:

- 1. Insufficient analysis of the influence of underground mining activities on the surface soil moisture in mining areas at the mine scale.
- 2. The selection of data uses medium- and lowresolution data to study the surface environment of the mine and lacks high-resolution remote sensing data for use at the mine scale.
- 3. At present, there is a lack of research on the scale effect of mining areas, and the scale of previous studies is relatively large.

Therefore, the specific objectives of our study are to:

1. Based on the three-period satellite data, the Scaled Soil Moisture Monitoring Index (S-SMMI) based on the NIR-Red feature space was used to analyze the differences in soil moisture between mining areas and non-mining areas, and the impact of underground mining activities on surface moisture in the mining area was analyzed from the scale of mines.

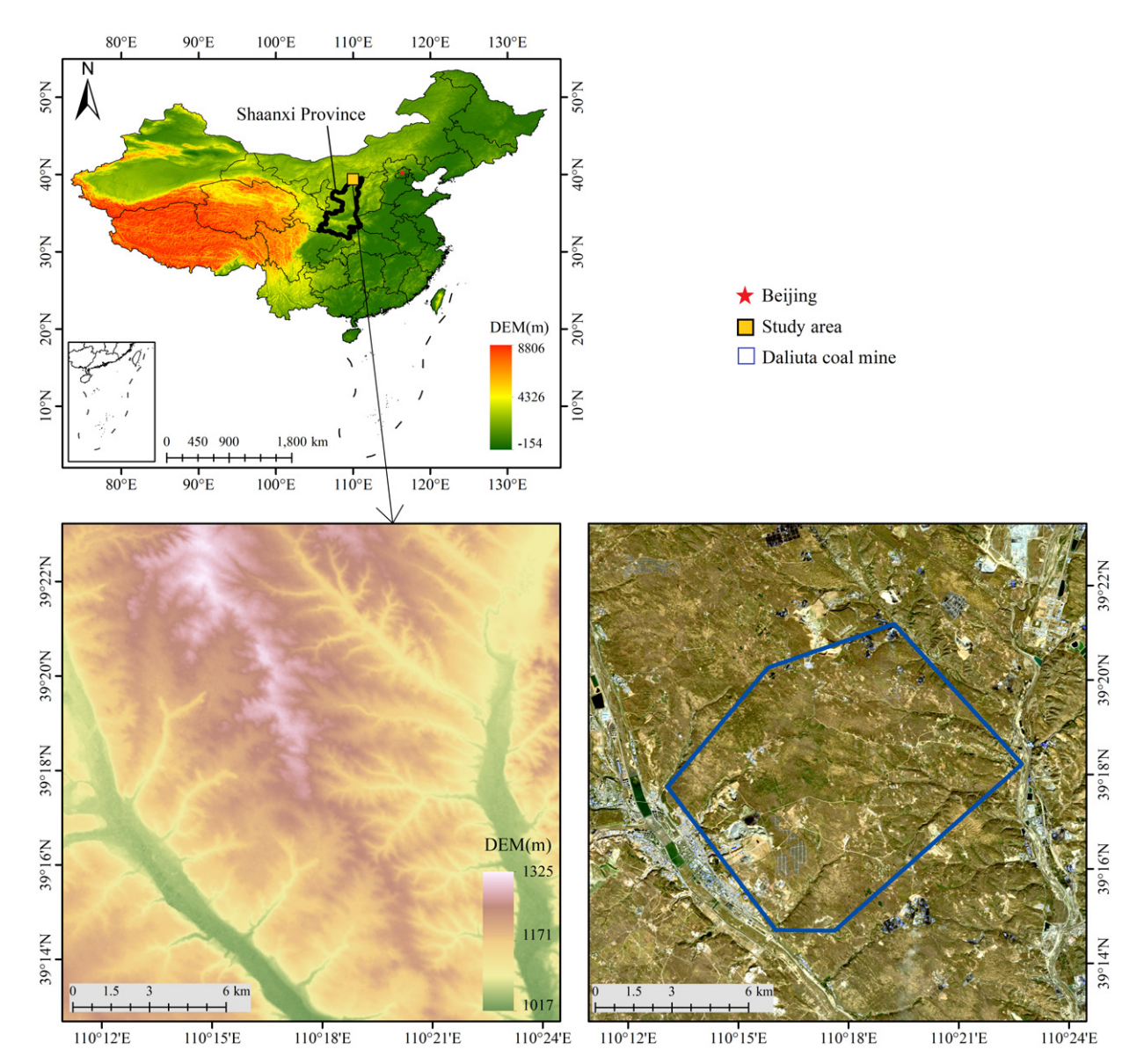


Figure 1: The geographical location of the Daliuta coal mine.

To study the scale effect of using S-SMMI to monitor soil moisture in the Daliuta coal mine under different scales.

2 Study Area

The Daliuta Coal Mine was established in October 1987 and went into production in 1996. The mine is located approximately 52.5 km northwest of Shenmu County on the edge of the Mu Us Desert, the center of the hinterland of the Dongsheng Coal Mine (38°52′N-39°41′N, 109°51′E-110°46′E) (Figure 1). Daliuta Coal Mine is the first modern coal mine in the world with annual output of 33×10⁶ t/a.

The stratigraphic structural unit in the study area belongs to the Ordos Block of North China Platform. Most of them are Triassic, Jurassic and Tertiary sedimentary strata, and Quaternary is all over the region which covered with deposits such as aeolian sand and the unconsolidated Sara Wusu Formation aquifer. Daliuta Coal Mine mainly mines No.1⁻², No.2⁻² and No.5⁻² coal seams of the Jurassic Yan'an Formation, and the average depth of the coal seam is approximately 150 m [32, 33]. The coal mine terrain is high in the north and low in the south, the north is a windy and sandy beach, and the south and west are typical Gaisa loess hilly landform areas, with an elevation of 1000 to 1250 m. It is a semi-arid continental monsoon climate in the temperate zone, characterized by long and cold win-

ters. The average annual wind speed is 2.3 m/s, and the maximum wind speed is 28.0 m/s. The types of land cover are mostly sandy land, shrubbery land, natural grassland, bare rock, fixed sandy land, and sand dune lowland. The lack of water resources in the study area and the fragile ecological environment are one of the unfavourable conditions that limit the development of large-scale coal resources in the area.

3 Methods

3.1 Data

Data used in this research are SPOT5 from October 16, 2010, and September 28, 2013; SPOT6 from October 5, 2015; Worldview-2 from 2015 September 12, 2015.

3.2 Image processing

Using the calibration coefficients of SPOT 6 remote sensing image for radiometric calibration, the original pixel DN value is converted into apparent radiance through sensor calibration. The FLAASH Atmospheric Correction Module was used in ENVI 5.1 to complete atmospheric calibration of the radiometrically calibrated image. Since the SPOT 5 image pixel values are 16-bit positive integers, they are converted into 8-bit storage format in Photoshop and then radiometrically scaled using gain offset coefficients. The calculation formula is:

$$L = \frac{DN}{Gains} + Bias \tag{1}$$

where *DN* is the value of the original image, Gains is the gain value of the remote sensing image; Bias is the offset, and the offset of each band is 0. Each band gain value is shown in Table 1. We perform a layer overlay and convert into BIL format to complete atmospheric correction of SPOT5 imagery.

Table 1: SPOT 5 data band gain value.

Band	Green	Red	NIR	SWIR
2010.10.16	0.36860	0.35956	0.33653	0.09494
2013.09.28	0.51537	0.46372	0.43206	0.12397

The Worldview-2 image needs to convert the DN value into the spectral radiance value of the entrance pupil of the sensor before atmospheric correction. We first convert the cell DN value into band integrated radiance

 $L_i(W \cdot m^{-2} \cdot sr^{-2})$ and calculate the spectral radiance $L(W \cdot m^{-2} \cdot sr^{-1} \cdot um^{-1})$.

$$L_i = DN \cdot absCalFactor \tag{2}$$

$$L = L_i/\Delta\lambda \tag{3}$$

where the *absCalFactor* is the absolute scaling factor, which is the effective width of the image band (um), Both of the above values can be found in the *.IMD file (Table 2).

Table 2: Worldview-2 Absolute Calibration Factor and Effective Width for Fach Band.

Band	Green	Red	NIR	SWIR
Absolute	0.0126	0.0971	0.0110	0.0122
calibration				
Effective width	0.0543	0.0630	0.0574	0.0989

The experimental image contains three different sensors. The remote sensing images acquired by different sensors have different projection information and will produce different degrees of geometric distortion during the acquisition. Therefore, the experiment uses a Worldview-2 image as the reference image to complete the image matching. The Image Registration workflow completes the geometric registration of other images.

According to the 2013 DWG format file of the Daliuta Coal Mine, the coordinated translation conversion in AUTOCAD converts it to WGS84 coordinates with the translation of east coordinates of 400066 and north coordinates of 4298218. However, the translation result still lacks projection information, so the output is opened in ArcGIS in .shp format and the projection is defined. Then, we create a file geodatabase and create a new line feature class. We manually highlight and save the 2013 Daliuta mining area in the .shp data during editing. Due to the lack of 2015 data, the mining area boundary in 2013 will use the 2013 mining area vector.

3.3 SMMI Index Construct

The Soil Moisture Monitor Index (SMMI) uses the distance from any point in the NIR-Red two-dimensional spectral feature space to the origin to characterize the soil moisture status in the study area. It is a soil moisture monitoring

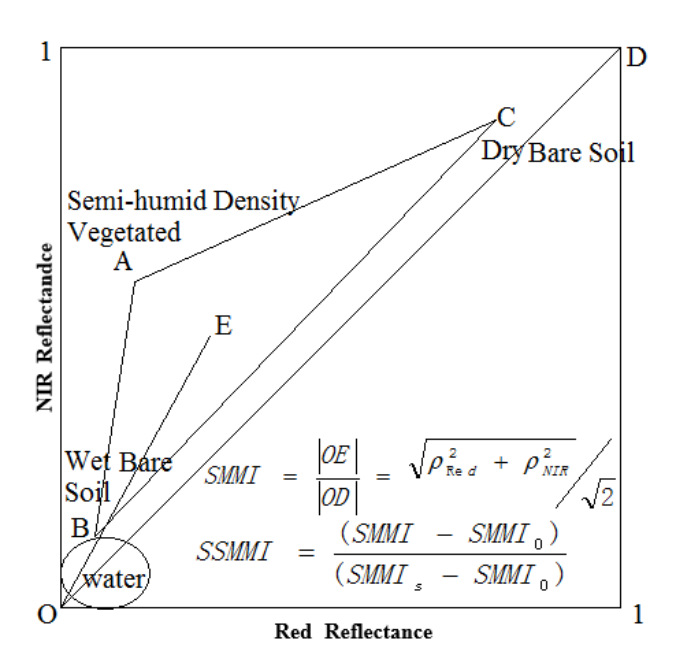


Figure 2: Sketch map of Scaled Soil Moisture Monitoring Index (SSMMI).

index that does not depend on the soil background line.

$$SMMI = \frac{|OE|}{|OD|} = \sqrt{r_i^2 + r_j^2} / \sqrt{2}$$
 (4)

where r_i , r_j is the surface reflectivity of TM/ETM+ i-band and j-band respectively. For example, in the NIR-Red twodimensional spectral feature space, i=4 and j=3. In the NIR-Red space, the change of the |OE| distance reflects the change of the soil moisture to some extent (Figure 2). From the moist bare soil at point B to the semi-moisture full vegetation coverage at point A and to the dry bare soil at point C, the soil moisture shows a decreasing trend. The distance from any point E to O in the two-dimensional feature space can explain the change of soil moisture. When point E is at point B, |OE| is the minimum and the soil moisture is the highest. When point E is at point C, |OE| is the maximum, and the soil moisture is the minimum. Usually, space closest to the O point is a water body or a relatively humid area, and the space far from the O point is a relatively dry or lowvegetation vegetation coverage area.

3.4 Scaled SMMI Index

To eliminate the phase difference, a scaled soil moisture monitoring index S-SMMI (scaled SMMI) was proposed above the soil moisture monitoring index SMMI.

$$S - SMMI = (SMMI - SMMI_0) / (SMMI_m - SMMI_0)$$
 (5)

where SMMI is the SMMI value corresponding to a pixel; $SMMI_0$ is the SMMI value corresponding to the saturated bare soil, and $SSMMI_m$ refers to the dry SMMI value. We select the SMMI value of $SMMI_0$ when the confidence rate of the cumulative frequency of SMMI in each image is 1%. When the cumulative frequency confidence is 99%, the corresponding SMMI value is $SSMMI_m$. The smaller the SSMMI value, then the greater the soil moisture content, because the S-SMMI value is negatively related to soil drought. Therefore, the 1-S-SMMI calculations were made to have a positive correlation for analysis, and the SPOT 6 soil moisture calculation results were resampled into a spatial resolution of 10 m for subsequent analysis.

4 Results

4.1 Analysis of the Temporal Change of Soil Moisture in the Daliuta Mining Area and Non-mining Area

As the mining progress continues to deepen, the average soil moisture in Daliuta has decreased between 2010 and 2015, both in the mining area and non-mining area (Figure 3). However, according to the standard for the classification of the humidity level, the soil moisture is in a wet state. In 2013, the soil moisture was generally higher than that in 2010 but it decreased again in 2015. On the whole, the average soil moisture in non-mining areas is greater than the mining area within the three periods.

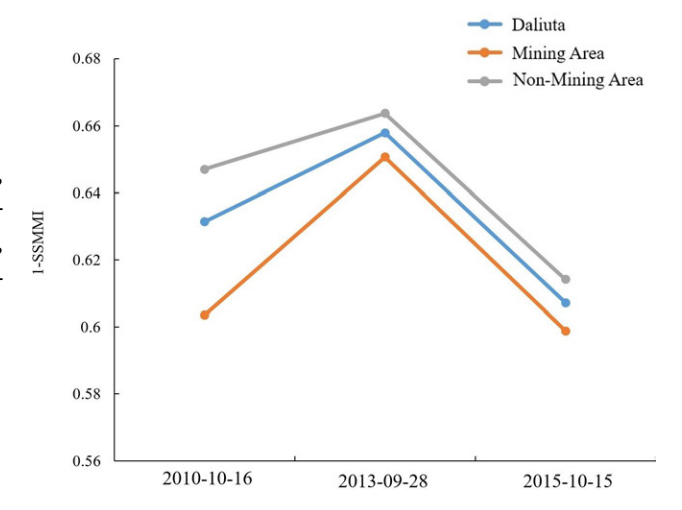


Figure 3: Variation of average soil moisture in Mining Area and non-mining area of Daliuta.

Time	Opencast mine		Vegetation		Sand		Water	
	Area(km²)	1-SSMMI	Area(km²)	1-SSMMI	Area(km²)	1-SSMMI	Area(km²)	1-SSMMI
2010.10.16	1.58	0.85	73.90	0.70	14.67	0.32	0.4	0.80
2013.09.28	2.27	0.79	74.24	0.71	11.30	0.40	0.03	0.97
2015.10.15	2.98	0.78	77.90	0.65	5.76	0.30	0.04	0.96

Table 3: The area of different underlying surfaces and the mean 1-SSMMI index.

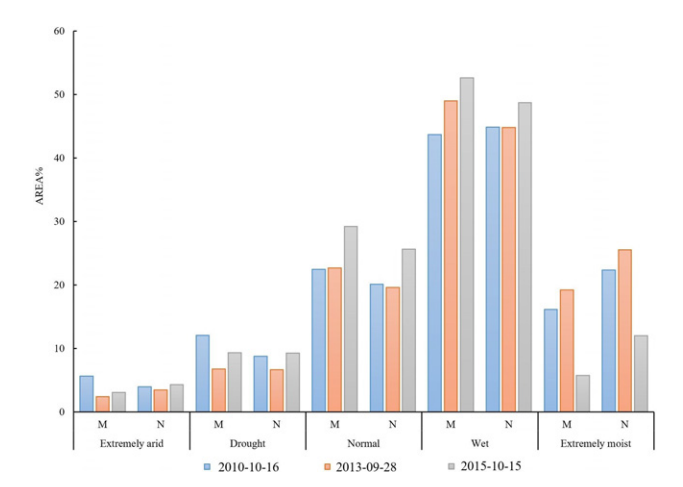


Figure 4: Changes in Soil Moisture at Different Levels in Daliuta Mining and Non-mining Areas.

4.2 Spatial Variation of Soil Moisture in Daliuta Mining Area and Non-mining Area

The soil moisture level classification criteria are: 1) when 0<S-SMMI≤ 0.2 is extremely arid; 2) when 0.2<S-SMMI≤ 0.4 is drought; 3) when 0.4<S-SMMI≤ 0.6 is normal; 4) when 0.6 < S- SMMI ≤ 0.8 is wet; 5) when 0.8 < S-SMMI ≤ 1 is extremely moist. The extremely arid area of the Daliuta mining area is decreasing; the area of non-mining areas is increasing, which has decreased and increased by 2.57% and 0.37%, respectively. The normal and wet soil moisture areas are increasing, and the increase rate of the mining areas is relatively large. From the year 2010 to 2015, the proportion of the wet soil area in the mining area increased by 15.7%. Extremely humid areas have a decreasing trend, in 2015, the proportions of normal, wet, and extremely humid areas in the Daliuta mining and non-mining areas were 87.62% and 86.42% respectively, of which the proportion of the mining area was 1.66% higher than that of the nonmining areas (Figure 4).

Figure 5 shows that, overall, the soil moisture in the northwest, middle, and southeast parts of the Dali Tower was mostly arid and extremely arid in 2010, and by 2015, its extremely arid area was significantly reduced. However,

the extremely wetted area also appeared within three years as a whole. There is a decreasing trend; the extremely arid area of the mining area is mainly distributed in the northeast and northwest. It can be seen from the figure that the extremely arid area of the mining area was significantly reduced from 2010 to 2015, and the area of the normal and wet soil increased. This is due to the result of the increase in the area of desert vegetation on the surface of the Daliuta coal mining area in 2010; from 2010 to 2015, the area of the drought in the north, southwest, and east of the nongrowing area continues to increase.

4.3 Analysis of Soil Moisture Changes in Different Underlying Surfaces of Daliuta

The maximum likelihood classification of the three remotely sensed images were done on ENVI. To improve the separability and classification accuracy of ROI, the image texture information, normalized vegetation index and S-SMMI were calculated before the classification, and the original image was superimposed onto it. In a new layer, we select five surfaces ROIs on the new layer as opencast mines, bodies of water, impervious layers, vegetation, sandy lands, and then generate random samples from the selected ROI. We use random samples to complete the new layer. Then, we perform Maximum Likelihood Classification and post-classification processing; the accuracy of the selected original ROI as a real surface sample is verified, and the overall classification accuracy and kappa coefficient of the classifications are recorded.

In the past three periods, the surface sand area of the Daliuta Coal Mine has decreased by 8.91 km² between 2010 and 2015, showing a gradual decrease, while the area of vegetation, and surface coal mines has increased to varying degrees. As seen in Table 2 and Figure 6, the average humidity in the water and sand areas tends to be stable, and the mean value of vegetation humidity shows a downward trend. This is because although the vegetation cover area increases, and the increased vegetation mostly grows in the sand, resulting in overall vegetation. With the decrease of the average humidity, the soil moisture of open-

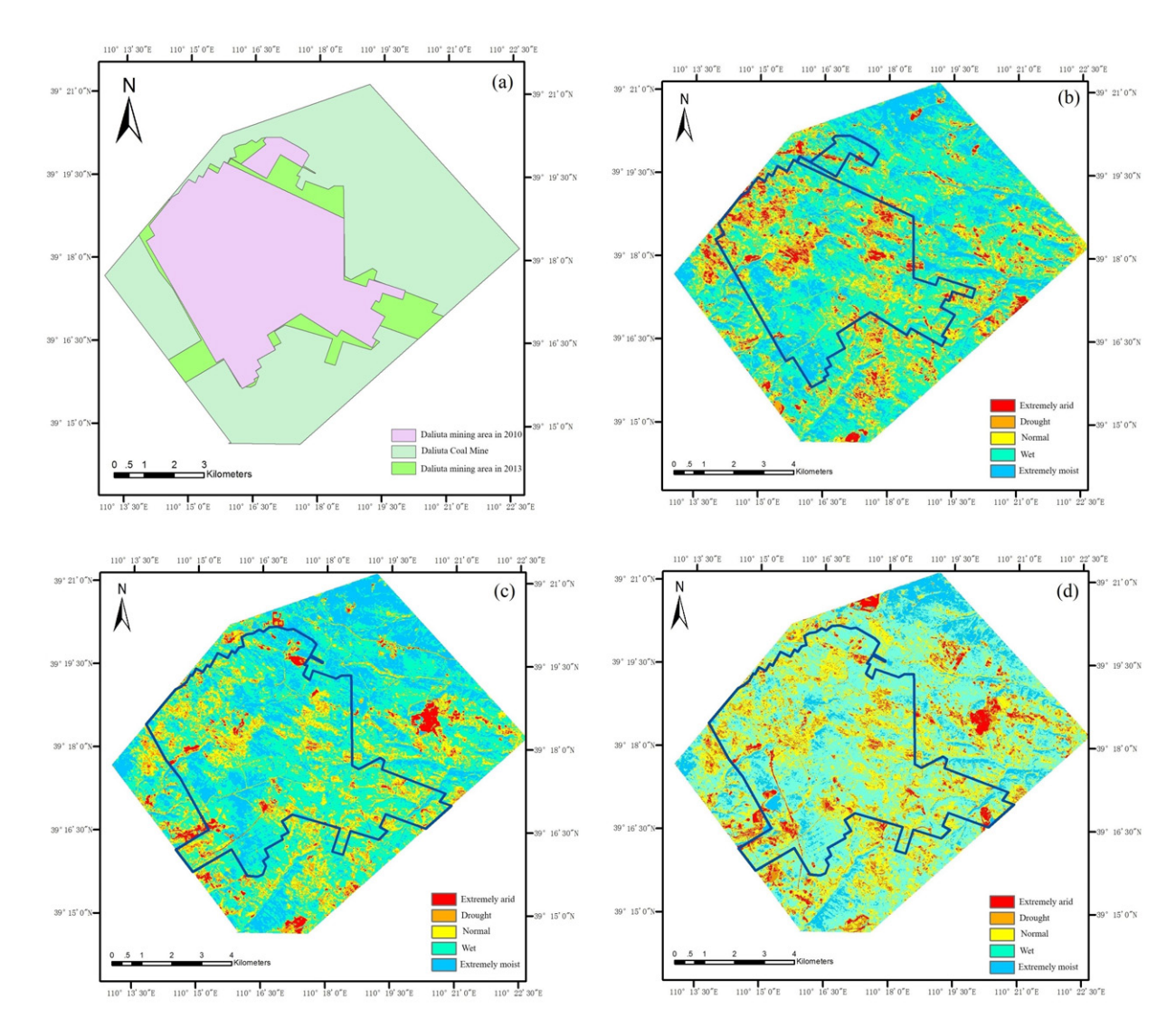


Figure 5: Spatial Distribution of 1-SSMMI Index of SPOT in Daliuta (a) in 2010(a), 2013(b) and 2015(c).

pit coal mines continues to decrease, but it is in a wet state in all three periods.

4.4 Remote Sensing Image Scale Conversion and Evaluation Index

After the ascending scale conversion, remote sensing data will inevitably lead to different levels of information loss or variation in the image. With different methods for scaling up, the loss of spectral information and feature information will also have different degrees of severity. To be able to quantitatively analyze the scale effect of the remote sensing data studied, the analysis indicators such as the mean value of the pixel, the standard deviation, the peak signal-to-noise ratio, the correlation coefficient, and the spectral

distortion are introduced to describe the scale effect between the studied scales.

 Calculating the average value of all the pixel values in the remote sensing image can express the mean value of the entire image, and obtaining the mean value in three different scales can intuitively explain the scale effect. Its expression is as follows:

$$E = \frac{1}{MN} \sum_{i=1}^{M} \sum_{j=1}^{N} f(i,j)$$
 (6)

where E is the average value of the pixel values in the entire image, M and N are the number of rows and columns of the pixels in the image and are the pixel values in the i row and the j column.

2. We calculate the Standard deviation. The standard deviation describes the degree of deviation between

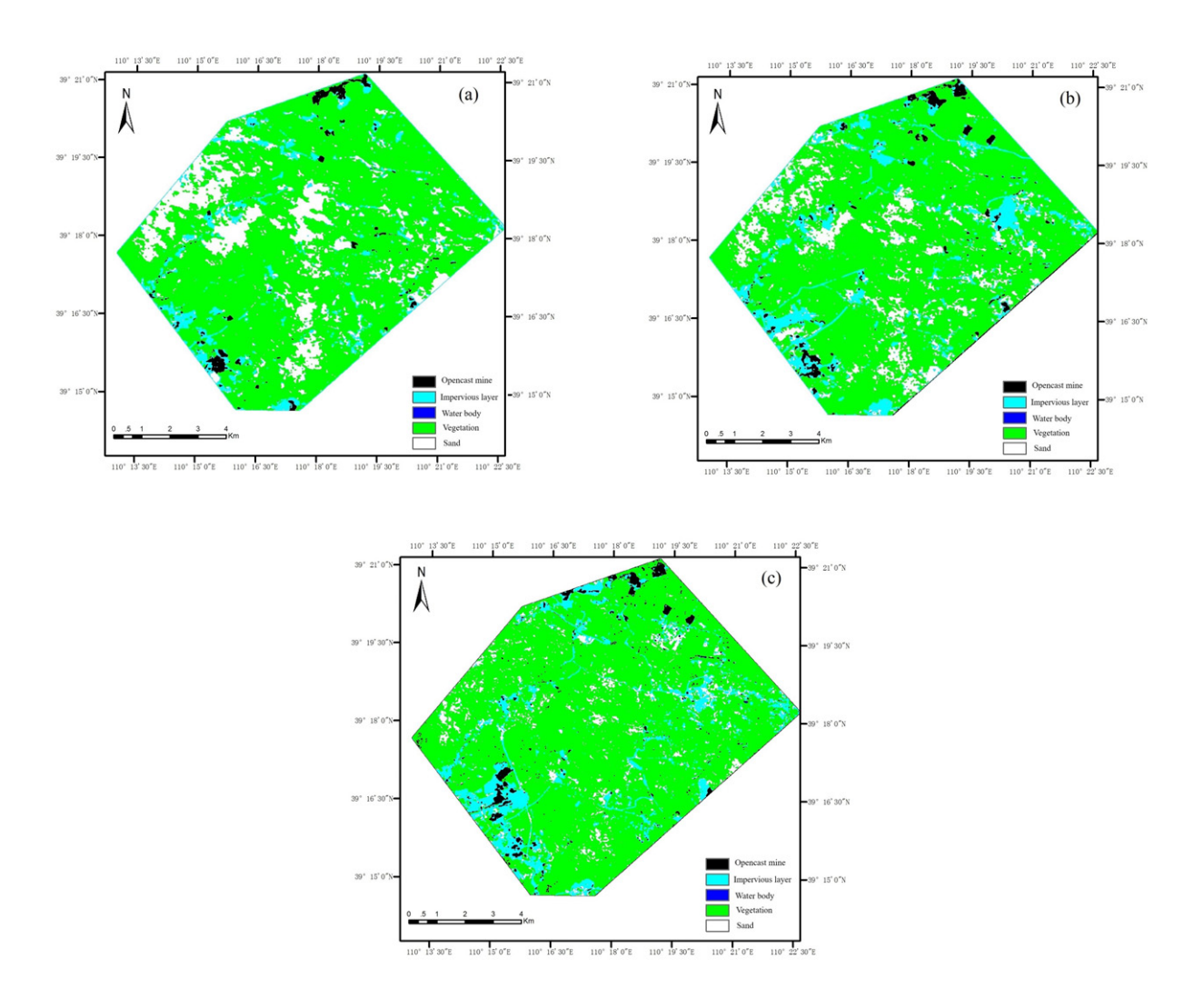


Figure 6: Classification results for 2010(a), 2013(b), and 2015(c).

the pixel value and the average value of the image before and after scaling. The larger the standard deviation, then the more dispersed the gray value of the image; the better the visual effect, the greater the amount of information covered, and the worse the visual effect. For the smaller the amount of information, the expression is as follows:

$$std = \sqrt{\frac{1}{MN - 1} \sum_{i=1}^{M} \sum_{j=1}^{N} f(i, j)}$$
 (7)

where M and N are the number of rows and columns of the pixels in the image and are the pixel values in the i row and the j column.

3. For the Peak Signal to Noise Ratio, the *PSNR* describes the maximum value of the image noise signal and can express the relationship between the vertex value and background noise. In general, *PSNR* is used to compare the difference between the image

before and after the scale conversion to express the degree of distortion after the image is transformed. The larger the peak signal-to-noise ratio, then the better the image quality and the better the fidelity is. For the *PSNR*, the expression is as follows:

$$PSNR = 10$$

$$\times \lg \left[\frac{255^{2}}{M \times N \sum_{i=1}^{M} \sum_{j=1}^{N} (f(i,j) - g(i,j))^{2}} \right]$$
(8)

where PSNR is the peak signal-to-noise ratio, f(i, j) and g(i, j) are pixel values before and after scaling.

4. We calculate the Spectral distortion. Spectral distortion describes the distortion of the upscaled spectrum of a remote sensing image. The larger the value, then more image loss occurs.

It is truly larger, but the difference is less, and the formula is as follows:

$$D = \frac{1}{MN} \sum_{i=1}^{M} \sum_{j=1}^{N} |f(i,j) - g(i,j)|$$
 (9)

where f(i, j) and g(i, j) indicates the pixel values before and after the remote sensing image transformation.

The 1-SSMMI mean values are basically the same at spatial resolutions of 2 m, 6 m, and 30 m. Table 4 shows that as the scale increases, the mean 1-SSMMI of the image shows a decreasing trend, but the change is very small, and the average soil moisture from the 2 m scale to the 30 m scale only decreased by 0.0016. This shows that the soil moisture information in the 2 m to 30m scale conversion is basically unchanged. The standard deviation of 1-SSMMI is the smallest in the 2 m scale, and the standard deviation is in the middle of 6 m, while the standard deviation of 30m is the largest. This shows that the image covers more information as the scale increases.

Table 4: The mean and standard deviation of three scales 1-SSMMI.

Index	2m	6m	30m
mean value of the pixel	0.5694	0.5693	0.5678
Standard deviation	0.1872	0.1874	0.1888

Table 5: The PSNR and Spectral distortion of three scales 1-SSMMI.

Index	2m to 6m	6m to 30m	2m to 30m
PSNR	70.5707	65.4526	65.3457
Spectral	0.00008	0.00015	0.00016
distortion			

Table 5 shows that when 2 m rise to 6 m, PSNR is the largest, and 6 m rises to 30 m, while 2 m rise to 30 m. This shows that from the point of view of fidelity, the 1-SSMMI distortion is the lowest and the fidelity is high in the first rise scale (Figure 7). The degree of 1-SSMMI distortion in the second elevation scale is the middle, and the 1-SSMMI distortion of the third rising scale is the most serious and the fidelity is poor. The spectral distortion produced by the 2m~6m scale conversion is the least, the spectral distortion produced by the 6m~30m scale conversion is the second, and the spectral distortion produced by the 2m~30m scale conversion is the most serious (Figure 8). This indicates that the larger the scale difference is, the more sig-

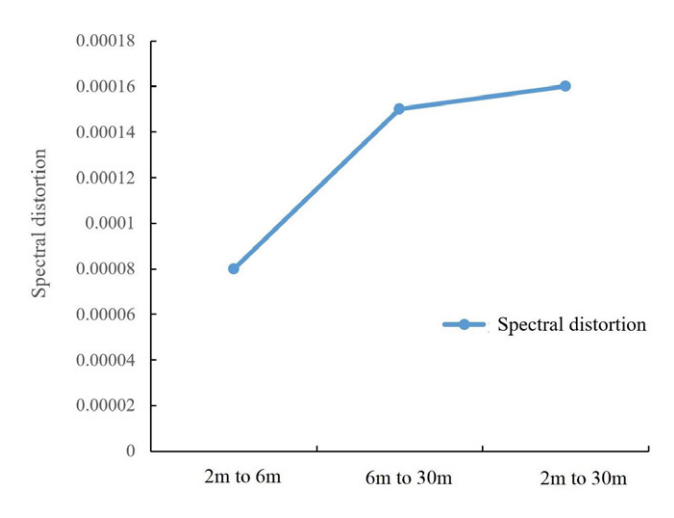


Figure 7: Spectral Distortion of 1-SSMMI Between Three Scale Conversions.

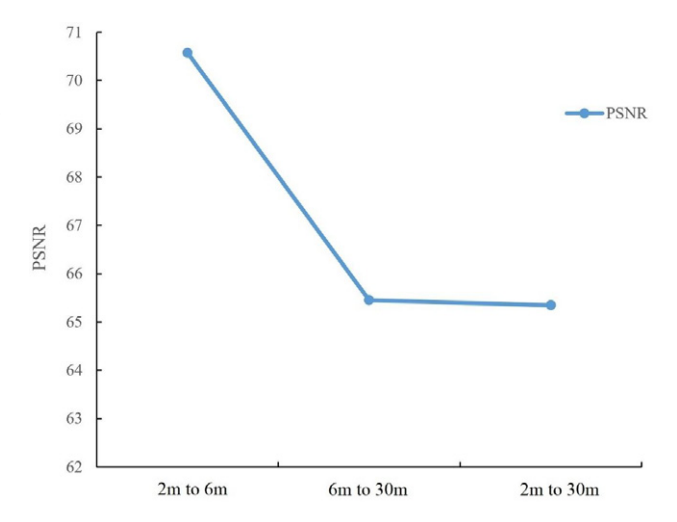


Figure 8: PSNR Statistics of 1-SSMMI Between Three Scale Conversions.

nificant the spectral distortion is, then the more severe the scale effect is.

5 Discussion

The Daliuta coal mine is the earliest mine built in Shendong Mining Area. It is located in arid and semi-arid desertification areas with fragile ecological environment. Therefore, it is of great significance to study the influence of underground mining disturbance activities on the ecological environment by studying the surface soil moisture of coal mines. Due to the rational exploitation of coal mines and the emphasis on ecological environment protection in recent years, the overall surface soil moisture in the Daliuta coal mining area in 2015 has turned better than that

in 2010, but the proportion of extremely wet area is still decreasing, and the proportion of extremely dry area in non-mining area is showing a growing trend. The main reason is that the mining activities in coal mining face have destroyed the stability of the ground vegetation and soil, reduce its resistance and recovery ability to environmental impact [33–35]. The vegetation coverage of the mining area has increased year by year, but the soil is seriously eroded [36–39]. Thus, although the vegetation coverage is increasing in the mining area, the soil stability type is destroyed, which results in the reduction of the extremely wet area of soil moisture.

Based on the resampling method, the scale-up conversion of Worldview-2 scale soil moisture data was carried out. The scale-up scales were 2m~6m, 6m~30m, and 2m~30m, respectively. The scale effects of soil moisture between 2m, 6m, and 30m were analyzed. Four evaluation factors, average value, standard deviation, peak signal-to-noise ratio (PSNR) and spectral distortion, were used to make a detailed analysis. Among the three scales, the larger the scale, the more serious the distortion degree and distortion degree of soil moisture information, and the more obvious the scale effect of soil moisture information changes with the scale.

6 Conclusion

The Daliuta coal mine is the earliest mine in the Shendong mining area. It is located in arid and semi-arid desert areas and has a fragile ecological environment. Therefore, it is of great significance to study the influence of underground mining disturbance on the ecological environment of the Daliuta mine by studying the surface soil moisture elements. The main conclusions were drawn through this study are as follows:

- 1. The average soil moisture in the Daliuta mine is in descending order of average soil moisture in the nongrowing area > average soil moisture in the Daliuta mine> average soil moisture in the mining area, and the ratio of extremely arid, dry, and extremely moist areas in the coal mine has been reduced to varying degrees. The normal and wet areas have increased by 11.86%.
- 2. Between 2010 and 2013, the proportion of extremely arid and arid area in the mining area has decreased rather than the non-mining area, which shows an increasing trend. In 2015, the proportion of normal, wet, and extremely moist areas in the mining area is 1.66% more than that in the non-mining area.

3. During scale conversions, the average soil moisture change was small, and the average soil moisture value from the 2m scale to 30m was only reduced by 0.0016. In the scale conversions, the larger the scale of conversion, the more severe the degree of distortion and distortion of soil moisture information.

Acknowledgement: This research was funded by the project of Key Laboratory of Mine Geological Hazards Mechanism and Control (6000180096 and KF2018-04), the National Natural Science Foundation of China (Grant No. 41401496) and Xi'an University of Science and Technology (No. 2019YQ3-04).

References

- [1] Wang, Lingli, and J. J. Qu. Satellite remote sensing applications for surface soil moisture monitoring: A review. Frontiers of Earth Science in China, 2009,3(2),237-247, DOI:10.1007/s11707-009-0023-7
- [2] Zhang, Dianjun, et al. Validation of a practical normalized soil moisture model with in situ measurements in humid and semi-arid regions. International Journal of Remote Sensing, 2015,36(19-20),5015-5030, DOI:10.1080/01431161.2015.1055610
- [3] Liang, Wei Li, et al. Spatial structure of surface soil water content in a natural forested headwater catchment with a subtropical monsoon climate. Journal of Hydrology, 2014,516(4),210-221, DOI: 10.1016/j.jhydrol.2014.01.032
- [4] Awe, G. O., et al. Temporal processes of soil water status in a sugarcane field under residue management. Plant and Soil,2015,387(1-2),395-411, DOI:10.1007/s11104-014-2304-5
- [5] Lin, H. Earth's Critical Zone and hydropedology: concepts, characteristics, and advances. Hydrology and Earth System Sciences, 2010,6(2), 3417-3481, DOI:10.5194/hess-14-25-2010
- [6] Peng, Jian, et al. Spatial Downscaling of Satellite Soil Moisture Data Using a Vegetation Temperature Condition Index. IEEE Transactions on Geoscience and Remote Sensing, 2015, 54(1),558-566, DOI: 10.1109/TGRS.2015.2462074
- [7] Istanbulluoglu, Erkan, and R. L. Bras. On the dynamics of soil moisture, vegetation, and erosion: Implications of climate variability and change. Water Resources Research, 2006,42(6),650-664, DOI:10.1029/2005WR004113
- [8] Houser, Chris A. Soil Moisture: A central and unifying theme in Physical Geography. Progress in Physical Geography, 2008,35(1),65-86, DOI:10.1177/0309133310386514
- [9] Seneviratne, Sonia I., et al. Investigating soil moisture-climate interactions in a changing climate: A review. Earth Science Reviews, 2010,99(3),125-161, https://doi.org/10.1016/j.earscirev. 2010.02.004
- [10] Romano, Nunzio. Soil moisture at local scale: Measurements and simulations. Journal of Hydrology, 2014,516(6),6-20, DOI: 10.1016/j.jhydrol.2014.01.026
- [11] Peng, J, J. Niesel, and A. Loew. Evaluation of soil moisture down-scaling using a simple thermal-based proxy -the REMEDHUS net-

- work (Spain) example. Hydrology and Earth System Sciences Discussions, 2015,12(8),8505-8551, DOI:10.5194/hess-19-4765-2015
- [12] Petropoulos, George P., G. Ireland, and B. Barrett. Surface soil moisture retrievals from remote sensing: Current status, products & future trends. Physics and Chemistry of the Earth Parts A/b/c s, 2015,83–84, 36-56, DOI:10.1016/j.pce.2015.02.009
- [13] Loew, A., R. Ludwig, and W. Mauser. Derivation of surface soil moisture from ENVISAT ASAR wide swath and image mode data in agricultural areas. IEEE Transactions on Geoscience and Remote Sensing, 2006, 44(4),889-899, DOI:10.1109/tgrs.2005.863858
- [14] Toby, Carlson. An Overview of the "Triangle Method" for Estimating Surface Evapotranspiration and Soil Moisture from Satellite Imagery. Sensors, 2007,7(8),1612-1629, DOI:10.3390/s7081612
- [15] Sandholt, Inge, K. Rasmussen, and J. Andersen. A simple interpretation of the surface temperature/vegetation index space for assessment of surface moisture status. Remote Sensing of Environment, 2002,79(2). 213-224, DOI:10.1016/s0034-4257(01)00274-7
- [16] Wagner, Wolfgang, *et al.* Operational readiness of microwave remote sensing of soil moisture for hydrologic applications. Water Policy, 2007,38(1),1-20, DOI:10.2166/nh.2007.029
- [17] Zribi, M., et al. Influence of Radar Frequency on the Relationship Between Bare Surface Soil Moisture Vertical Profile and Radar Backscatter. IEEE Geoscience and Remote Sensing Letters, 2013,11(4),848-852, DOI:10.1109/LGRS.2013.227989
- [18] Liu, Y. Y, et al. Developing an improved soil moisture dataset by blending passive and active microwave satellite-based retrievals. Hydrology and Earth System Sciences, 2014,15(2),425-436, DOI:10.5194/hess-15-425-2011
- [19] Anne, Naveen J. P., et al. Modeling soil parameters using hyperspectral image reflectance in subtropical coastal wetlands. International Journal of Applied Earth Observations and Geoinformation, 2014,33(33),47-56, DOI:10.1016/j.jag.2014.04.007
- [20] Pan, Ming, A. K. Sahoo, and E. F. Wood. Improving soil moisture retrievals from a physically-based radiative transfer model. Remote Sensing of Environment, 2014,140(1),130-140, DOI:10.1016/j.rse.2013.08.020
- [21] Bogena, H. R., *et al.* Evaluation of a low-cost soil water content sensor for wireless network applications. Journal of Hydrology, 2007,344(1),32-42, DOI: 10.1016/j.jhydrol.2007.06.032
- [22] Top, G Clarke, and W. D. Reynolds. Time domain reflectometry: a seminal technique for measuring mass and energy in soil. Soil and Tillage Research, 1998,47(1–2), 125-132, DOI:10.1016/s0167-1987(98)00083-x
- [23] Zhang, Dianjun, and G. Zhou. Estimation of Soil Moisture from Optical and Thermal Remote Sensing: A Review. Sensors, 2016,16(8).1308, DOI:10.3390/s16081308
- [24] Kahle, Anne B. A simple thermal model of the Earth's surface for geologic mapping by remote sensing. Journal of Geophysical Research, 1977,82(11).1673-1680, DOI:10.1029/JB082i011p01673
- [25] Price, J. C. On the analysis of thermal infrared imagery: the limited utility of apparent thermal inertia. Remote Sensing of Environment, 1985,18(1).59-73, DOI:10.1016/0034-4257(85)90038-0

- [26] Moran, M. S., *et al.* Estimating crop water deficit using the relation between surface-air temperature and spectral vegetation index. Remote Sensing of Environment:an interdisciplinary journal, 1994,49(3), 246-263
- [27] Ghulam, Abduwasit, Q. Qin, and Z. Zhan. Designing of the perpendicular drought index. Environmental Geology, 2007,52(6),1045-1052, DOI:10.1007/s00254-006-0544-2
- [28] Ghulam, Abduwasit, et al. Modified perpendicular drought index (MPDI): a real-time drought monitoring method. Isprs Journal of Photogrammetry and Remote Sensing, 2007,62(2), 150-164, DOI: 10.1016/j.isprsjprs.2007.03.002
- [29] Zhang, Bing, et al. Application of hyperspectral remote sensing for environment monitoring in mining areas. Environmental Earth Sciences, 2012,65(3), 649-658, DOI:10.1007/s12665-011-1112-y
- [30] Amani, Meisam, et al. Two new soil moisture indices based on the NIR-red triangle space of Landsat-8 data. International Journal of Applied Earth Observation and Geoinformation, 2016, 50, 176-186, DOI: 10.1016/j.jag.2016.03.018
- [31] Liu, Ying, L. Wu, and H. Yue. Biparabolic NDVI-Ts Space and Soil Moisture Remote Sensing in an Arid and Semi-arid Area. Canadian Journal of Remote Sensing, 2015, 41(3),159-169, DOI:10.1080/07038992.2015.1065705
- [32] Zhao, C., Jin, D., Geng, J. et al. Numerical Simulation of the Groundwater System for Mining Shallow Buried Coal Seams in the Ecologically Fragile Areas of Western China. Mine Water and the Environment. 2019, 38(158), https://doi.org/10.1007/s10230-018-0551-z
- [33] Wang Yuchen, Bian Zhengfu, Lei Shaogang, et al. Investigating spatial and temporal variations of soil moisture content in an arid mining area using an improved thermal inertia model. Journal of Arid Land, 2017, 9(5): 712–726, DOI: 10.1007/s40333-017-0065-8
- [34] Lei S G, Bian Z F, Daniels J L, et al. Spatio-temporal variation of vegetation in an arid and vulnerable coal mining region. Mining Science and Technology, 2010,20(3): 485-490, DOI:10.1016/s1674-5264(09)60230-1
- [35] Lei S G, Bian Z F, Daniels J L, *et al.* Improved spatial resolution in soil moisture retrieval at arid mining area using apparent thermal inertia. Transactions of Nonferrous Metals Society of China, 2014,24(6): 1866–1873, DOI:10.1016/S1003-6326(14)63265-9
- [36] Yang D J, Bian Z F, Lei S G. Impact on soil physical qualities by the subsidence of coal mining: A case study in Western China. Environmental Earth Sciences, 2016,75(8): 652, doi: 10.1007/s12665-016-5439-2.
- [37] He Y, He X, Liu Z, et al. Coal mine subsidence has limited impact on plant assemblages in an arid and semi-arid region of northwestern China[J]. Ecoscience, 2017, 24(3-4), 1-13, https://doi.org/10.1080/11956860.2017.1369620
- [38] Liu Y. Vegetation and soil moisture monitoring by remote sensing in Shendong Mining Area. PhD Dissertation. Beijing: China University of Mining and Technology, 2013. (in Chinese)
- [39] Yongjun Y, Erskine P D, Shaoliang Z, et al. Effects of underground mining on vegetation and environmental patterns in a semi-arid watershed with implications for resilience management[J]. Environmental Earth Sciences, 2018, 77(17):605, DOI:10.1007/s12665-018-7796-5